Constants

$R = 2634\,\mathrm{km}$, $Q = 470\,\mathrm{GW}$ [Hay and Matsuyama, 2019], $Pr = 10$ [Kvorka and Čadek, 2022]. Soderlund [2019]: $\nu = 1.8{\cdot}10^{-6}\,\mathrm{m^2 s^{-1}}$, $\alpha = 2{\cdot}10^{-4}\,\mathrm{K^{-1}}$, $\rho = 1150\,\mathrm{kgm^{-3}}$, $\Omega = 10^{-5}\,\mathrm{s^{-1}}$, $C_p = 3500\,\mathrm{Jkg^{-1}K^{-1}}$, $g_o = 1.4\,\mathrm{ms^{-2}}$.

1 Radius ratio: 0.80

$$Ra = (6.00 \pm 0.50) Pr^{+1.13\pm0.02} Ek^{-2.16\pm0.03} Ra_Q^{0.58\pm0.01} \tag{1.1}$$

$$Ro = (0.33 \pm 0.05) Pr^{-0.10\pm0.02} Ek^{-0.23\pm0.03} Ra_Q^{0.37\pm0.01} \tag{1.2}$$

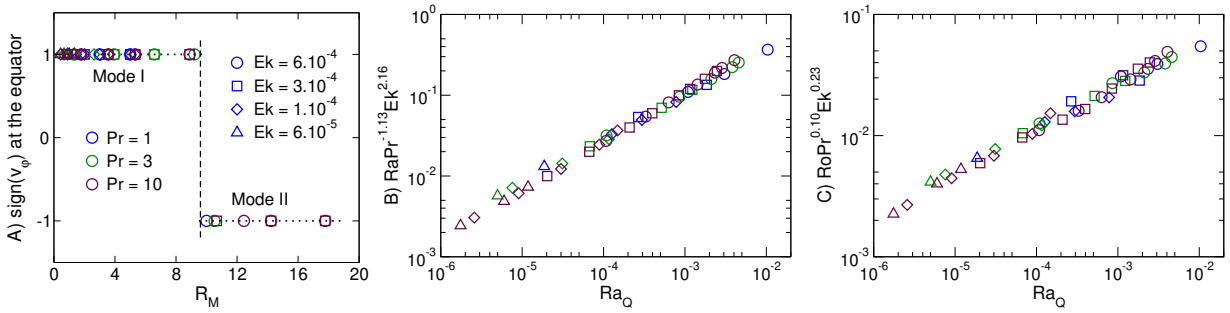

Figure 1.1: A) The sign of the zonal flow velocity on the outer boundary at the equator as a function of parameter $R_M = RaEk^{12/7}Pr^{-3/4}$. The overturn of equatorial zonal flow (vertical dashed line) is marked by $R_M \approx 9.6$. B) Graphs illustrating the scaling laws derived for Ra (Eq. 1.1) from the dataset in Table 1.2 using the least squares method. C) Graphs illustrating the scaling laws derived for Ro (Eq. 1.2) from the same dataset. Shapes and colors of the symbols indicate the values of parameters Ek and Pr used in the numerical simulation.

r_o [km]	D [km]	H [km]	Radius ratio	Ek	Ra_Q	Ra	U [m/s]
2629	518	5	0.80	$6.7{\cdot}10^{-13}$	$1.7{\cdot}10^{-9}$	$1.3{\cdot}10^{23}$	0.49
2608	493	26	0.81	$7.4{\cdot}10^{-13}$	$1.9{\cdot}10^{-9}$	$1.1{\cdot}10^{23}$	0.47

Table 1.1: Models of internal structure of Ganymede with aspect ratio close to 0.80 [Vance et al., 2018]. r_o is the outer radius of the ocean, D is the thickness of the ocean and H denotes the thickness of the ice shell. U is dimensional rms velocity (Eq. 1.2). The ocean is situated in the transitional regime regardless the ocean thickness (D), as $Ro_{loc} \approx 10^3$ and $Ro_c \approx 0.08$ in both cases. The flow geometry resembles Mode II, as $R_M \approx 31$ (see Fig 1.1A).

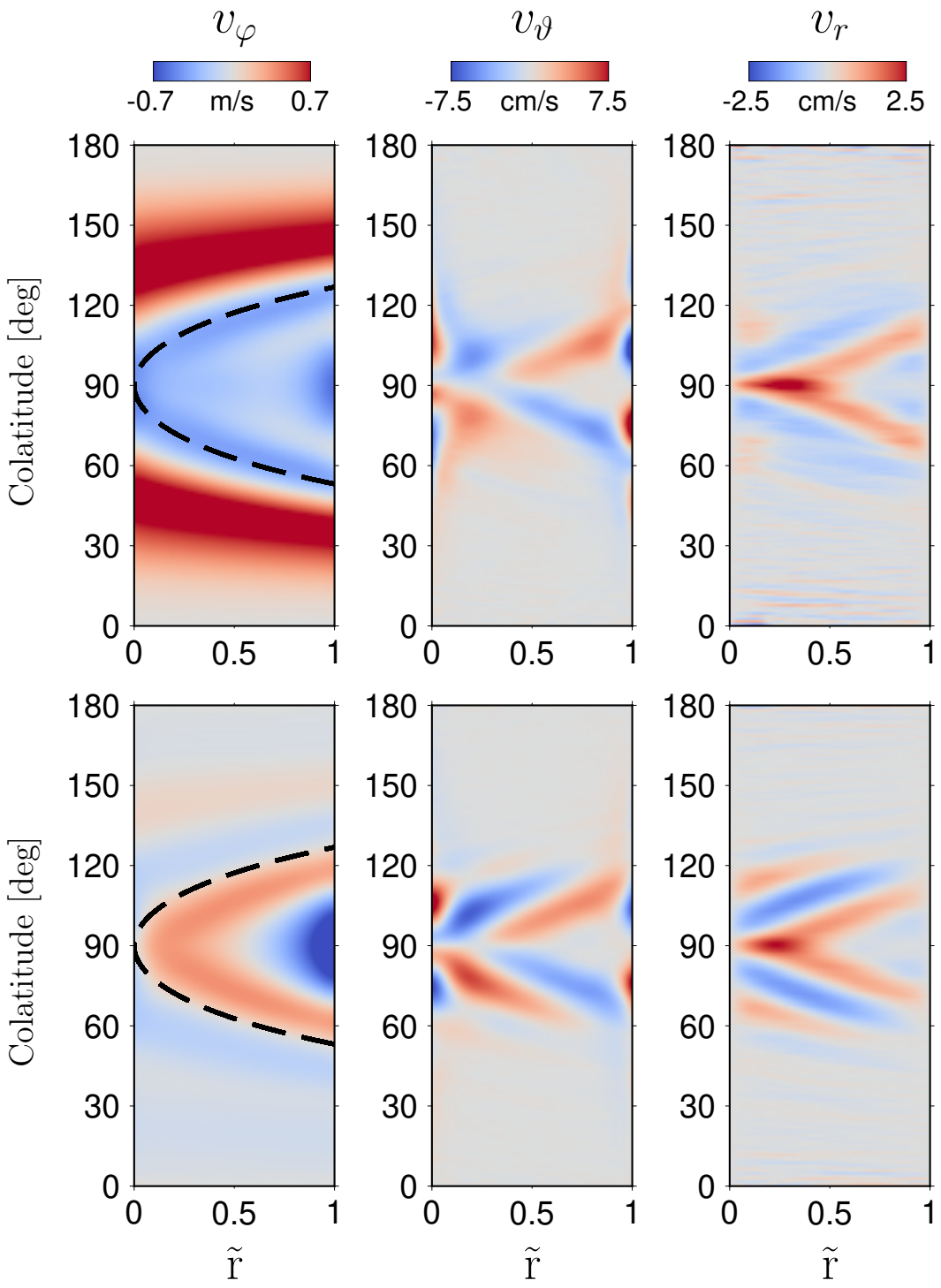

Figure 1.2: Forking of flow velocity pattern in Mode II for $Ek = 3{\cdot}10^{-4}$. The flow field is obtained for models No. 12,13 and is scaled so that $U = 0.49\,\mathrm{m/s}$ (see Table 1.1). The velocity fields are averaged over at least 0.02 viscous diffusion times and longitude. The x-axis is given in non-dimensional radius, $\tilde{r} = (r - r_i)/D$, where $r_i = r_o - D$. The dashed lines mark the position of the tangent cylinder (the cylinder with radius r_i whose axis is identical with the rotation axis).

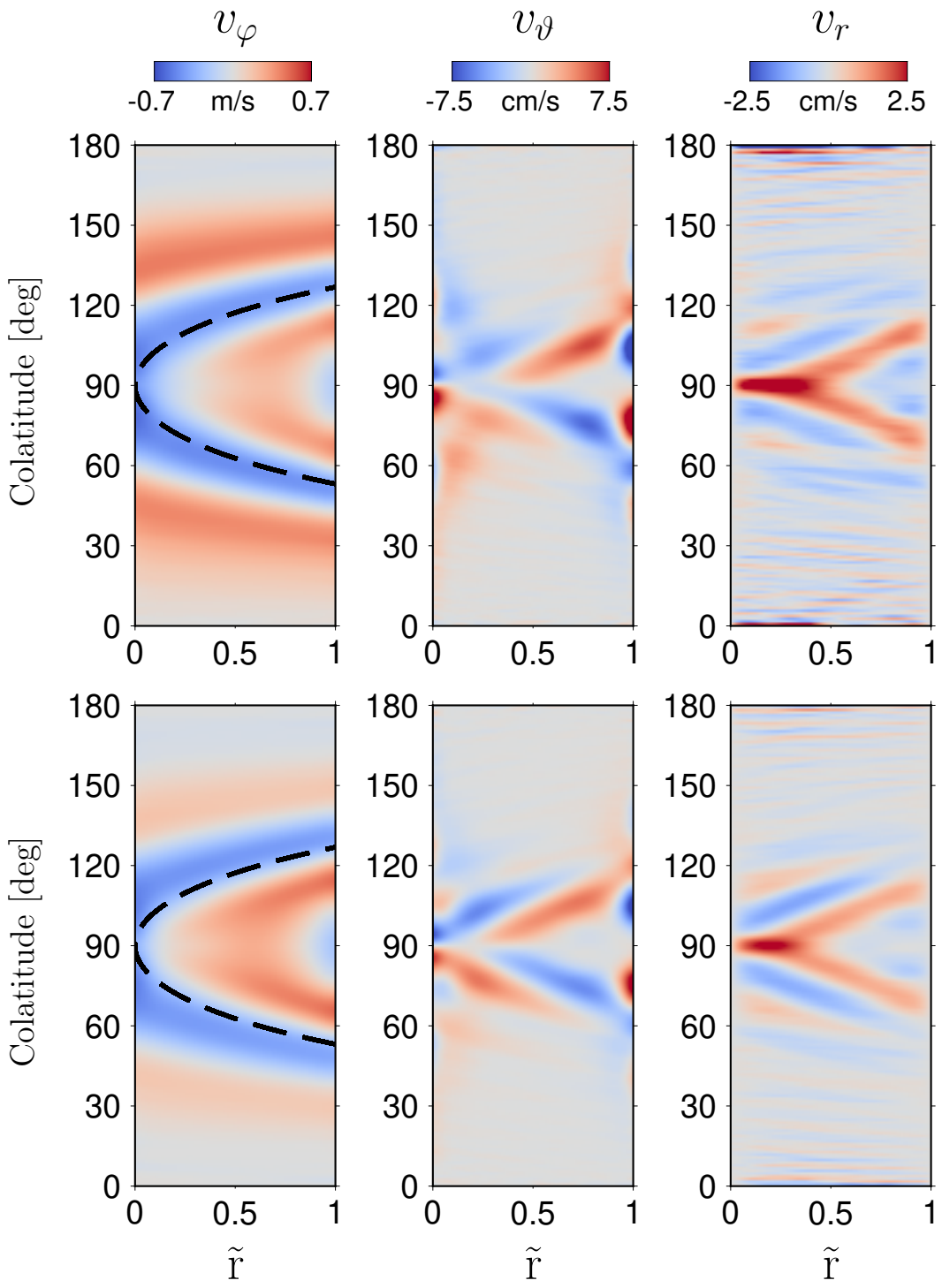

Figure 1.3: Forking of flow velocity pattern in Mode II for $Ek = 6{\cdot}10^{-4}$. The flow field is obtained for models No. 4,5 and is scaled so that $U = 0.49\,\mathrm{m/s}$ (see Table 1.1). The velocity fields are averaged over at least 0.02 viscous diffusion times and longitude. The x-axis is given in non-dimensional radius, $\tilde{r} = (r - r_i)/D$, where $r_i = r_o - D$. The dashed lines mark the position of the tangent cylinder (the cylinder with radius r_i whose axis is identical with the rotation axis).

Model No.	N_r	j_{max}	Pr	Ek	Ra	Ro_{loc}	Ro_c	R_M	Nu	Ro
0	61	159	10	$6{\cdot}10^{-4}$	$3.34{\cdot}10^{6}$	5.86	0.35	1.78	15.94	0.05
1	73	177	10	$6{\cdot}10^{-4}$	$6.67{\cdot}10^{6}$	11.73	0.49	3.56	23.87	0.07
2	73	177	10	$6{\cdot}10^{-4}$	$1.00{\cdot}10^{7}$	17.59	0.60	5.33	30.22	0.09
3	73	177	10	$6{\cdot}10^{-4}$	$1.67{\cdot}10^{7}$	29.32	0.77	8.89	40.83	0.13
4	85	213	10	$6{\cdot}10^{-4}$	$2.33{\cdot}10^{7}$	41.05	0.92	12.45	47.33	0.16
5	81	213	10	$6{\cdot}10^{-4}$	$2.67{\cdot}10^{7}$	46.91	0.98	14.23	50.61	0.18
6	79	213	10	$6{\cdot}10^{-4}$	$3.34{\cdot}10^{7}$	58.64	1.10	17.78	57.35	0.22
7	61	159	10	$3{\cdot}10^{-4}$	$5.47{\cdot}10^{6}$	3.17	0.22	0.89	14.76	0.03
8	67	177	10	$3{\cdot}10^{-4}$	$1.09{\cdot}10^{7}$	6.35	0.31	1.78	23.59	0.05
9	73	177	10	$3{\cdot}10^{-4}$	$2.19{\cdot}10^{7}$	12.70	0.44	3.56	36.34	0.07
10	73	177	10	$3{\cdot}10^{-4}$	$3.28{\cdot}10^{7}$	19.04	0.54	5.33	45.76	0.09
11	81	213	10	$3{\cdot}10^{-4}$	$5.47{\cdot}10^{7}$	31.74	0.70	8.89	58.09	0.13
12	85	237	10	$3{\cdot}10^{-4}$	$6.57{\cdot}10^{7}$	38.09	0.77	10.67	66.30	0.16
13	85	237	10	$3{\cdot}10^{-4}$	$8.76{\cdot}10^{7}$	50.78	0.89	14.23	75.42	0.18
14	89	297	10	$3{\cdot}10^{-4}$	$1.09{\cdot}10^{8}$	63.48	0.99	17.78	84.50	0.21
15	73	213	10	$1{\cdot}10^{-4}$	$1.80{\cdot}10^{7}$	1.80	0.13	0.44	15.36	0.02
16	73	213	10	$1{\cdot}10^{-4}$	$3.60{\cdot}10^{7}$	3.60	0.19	0.89	26.17	0.03
17	81	237	10	$1{\cdot}10^{-4}$	$7.20{\cdot}10^{7}$	7.20	0.27	1.78	42.64	0.05
18	89	285	10	$1{\cdot}10^{-4}$	$1.44{\cdot}10^{8}$	14.39	0.38	3.56	62.61	0.07
19	117	447	10	$1{\cdot}10^{-4}$	$2.16{\cdot}10^{8}$	21.59	0.46	5.33	69.72	0.10
20	81	237	10	$6{\cdot}10^{-5}$	$4.32{\cdot}10^{7}$	1.91	0.12	0.44	19.80	0.02
21	89	267	10	$6{\cdot}10^{-5}$	$8.64{\cdot}10^{7}$	3.81	0.18	0.89	33.12	0.03
22	97	317	10	$6{\cdot}10^{-5}$	$1.30{\cdot}10^{8}$	5.72	0.22	1.33	43.18	0.04
23	73	177	1	$6{\cdot}10^{-4}$	$1.00{\cdot}10^{6}$	7.00	0.60	3.00	6.03	0.17
24	85	213	1	$6{\cdot}10^{-4}$	$1.67{\cdot}10^{6}$	11.67	0.77	5.00	9.47	0.22
25	97	267	1	$6{\cdot}10^{-4}$	$3.34{\cdot}10^{6}$	23.35	1.10	10.00	15.43	0.30
26	85	237	1	$3{\cdot}10^{-4}$	$2.19{\cdot}10^{6}$	5.05	0.44	2.00	5.51	0.12
27	97	253	1	$3{\cdot}10^{-4}$	$5.47{\cdot}10^{6}$	12.64	0.70	5.00	13.50	0.18
28	85	237	1	$1{\cdot}10^{-4}$	$1.44{\cdot}10^{7}$	5.73	0.38	2.00	9.78	0.11
29	97	237	1	$1{\cdot}10^{-4}$	$2.16{\cdot}10^{7}$	8.60	0.46	3.00	14.69	0.13
30	97	267	1	$1{\cdot}10^{-4}$	$3.60{\cdot}10^{7}$	14.33	0.60	5.00	22.67	0.17
31	97	253	1	$6{\cdot}10^{-5}$	$1.73{\cdot}10^{7}$	3.04	0.25	1.00	6.00	0.06
32	73	177	3	$6{\cdot}10^{-4}$	$1.00{\cdot}10^{6}$	3.62	0.35	1.32	5.53	0.06
33	73	197	3	$6{\cdot}10^{-4}$	$3.00{\cdot}10^{6}$	10.87	0.60	3.95	12.86	0.13
34	85	213	3	$6{\cdot}10^{-4}$	$5.00{\cdot}10^{6}$	18.11	0.77	6.58	18.55	0.16
35	85	237	3	$6{\cdot}10^{-4}$	$7.00{\cdot}10^{6}$	25.36	0.92	9.21	23.70	0.19
36	97	267	3	$6{\cdot}10^{-4}$	$8.01{\cdot}10^{6}$	28.98	0.98	10.53	24.86	0.22
37	73	177	3	$3{\cdot}10^{-4}$	$3.28{\cdot}10^{6}$	3.92	0.31	1.32	7.89	0.06
38	85	213	3	$3{\cdot}10^{-4}$	$9.85{\cdot}10^{6}$	11.76	0.54	3.95	18.49	0.12
39	97	253	3	$3{\cdot}10^{-4}$	$1.64{\cdot}10^{7}$	19.61	0.70	6.58	25.95	0.16
40	73	213	3	$1{\cdot}10^{-4}$	$1.08{\cdot}10^{7}$	2.22	0.19	0.66	7.31	0.04
41	81	237	3	$1{\cdot}10^{-4}$	$2.16{\cdot}10^{7}$	4.45	0.27	1.32	13.97	0.06
42	97	253	3	$1{\cdot}10^{-4}$	$4.32{\cdot}10^{7}$	8.89	0.38	2.63	25.20	0.09
43	97	253	3	$6{\cdot}10^{-5}$	$2.59{\cdot}10^{7}$	2.36	0.18	0.66	9.03	0.03

Table 1.2: List of numerical simulations used to derive the scaling laws (Eqs. 1.1 and 1.2). Symbols N_r and j_{max} denote the number of the Chebyshev points and the cut-off degree used to discretize the governing equations in the radial and lateral directions, respectively. The results of the simulations are represented by the Nusselt (Nu) and Rossby (Ro) numbers.

2 Radius ratio: 0.85

$$Ra = (5.05 \pm 0.50) Pr^{+1.16 \pm 0.03} Ek^{-2.17 \pm 0.03} Ra_Q^{0.58 \pm 0.02} \tag{2.1}$$

$$Ro = (0.37 \pm 0.07) Pr^{-0.07 \pm 0.03} Ek^{-0.21 \pm 0.03} Ra_Q^{0.38 \pm 0.01} \tag{2.2}$$

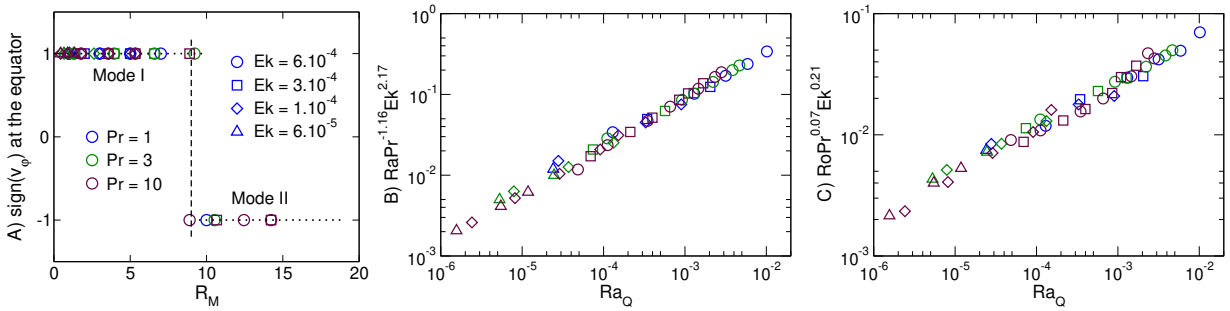

Figure 2.1: A) The sign of the zonal flow velocity on the outer boundary at the equator as a function of parameter $R_M = RaEk^{12/7}Pr^{-3/4}$. The overturn of equatorial zonal flow (vertical dashed line) is marked by $R_M \approx 9.0$. B) Graphs illustrating the scaling laws derived for Ra (Eq. 2.1) from the dataset in Table 2.2 using the least squares method. C) Graphs illustrating the scaling laws derived for Ro (Eq. 2.2) from the same dataset. Shapes and colors of the symbols indicate the values of parameters Ek and Pr used in the numerical simulation.

r_o [km]	D [km]	H [km]	Radius ratio	Ek	Ra_Q	Ra	U [m/s]
2564	361	70	0.86	$1.4{\cdot}10^{-12}$	$3.5{\cdot}10^{-9}$	$4.8{\cdot}10^{22}$	0.21

Table 2.1: Model of internal structure of Ganymede with aspect ratio close to 0.85 Vance et al. [2018]. r_o is the outer radius of the ocean, D is the thickness of the ocean and H denotes the thickness of the ice shell. U is dimensional root-mean-square velocity derived from the value of Ro, which is given by Eq. (2.2). The ocean is situated in the transitional regime of convection, as $Ro_{loc} \approx 10^3$ and $Ro_c \approx 0.10$. $R_M \approx 41$ places the ocean into Mode II.

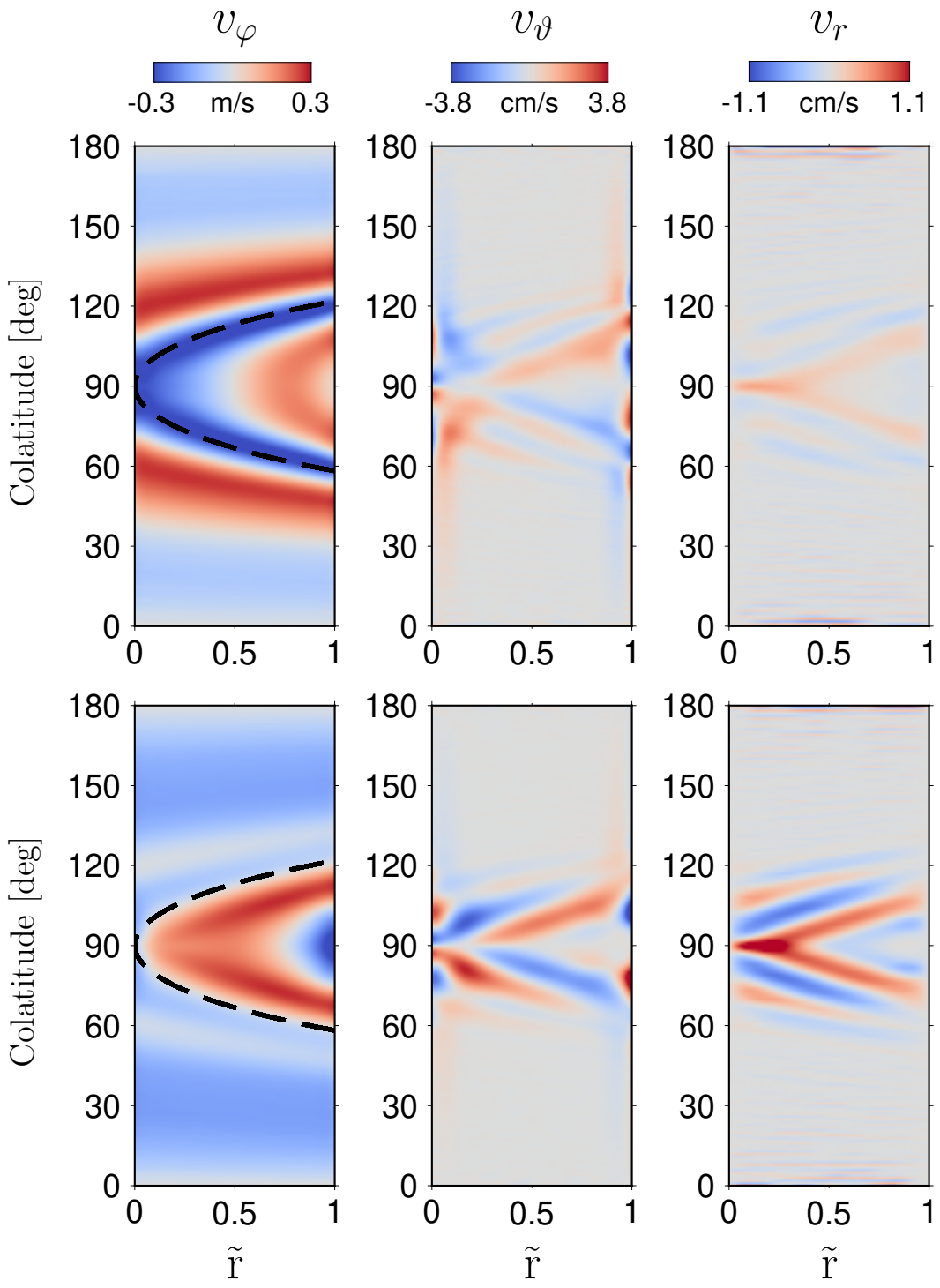

Figure 2.2: Forking of flow velocity pattern in Mode II for $Ek = 3{\cdot}10^{-4}$. The flow field is obtained for models No. 10 and 11 and is scaled so that $U = 0.21$ m/s (see Table 2.1). The velocity fields are averaged over at least 0.02 viscous diffusion times and longitude. The x-axis is given in non-dimensional radius, $\tilde{r} = (r - r_i)/D$, where $r_i = r_o - D$. The dashed lines mark the position of the tangent cylinder (the cylinder with radius r_i whose axis is identical with the rotation axis).

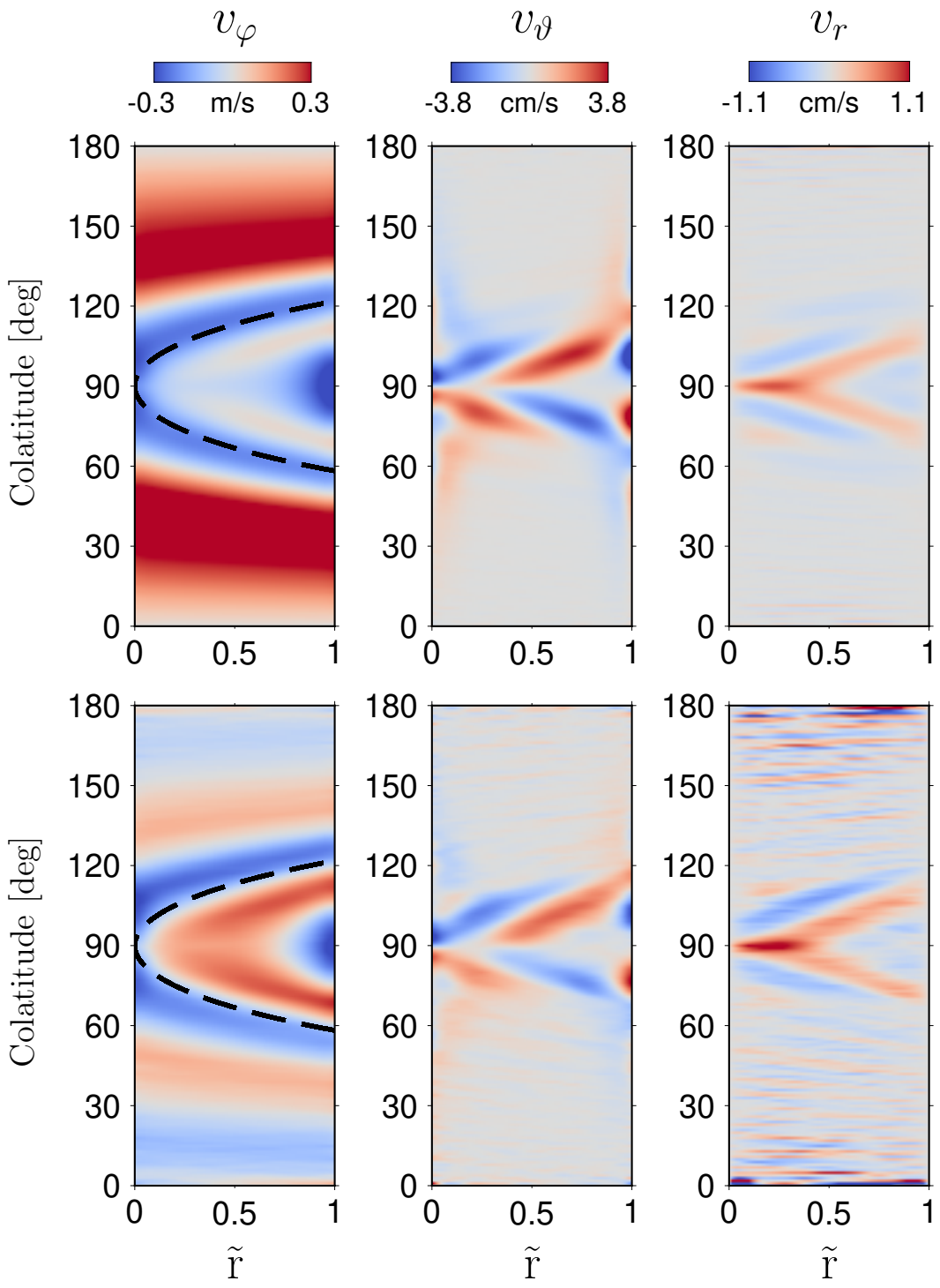

Figure 2.3: Forking of flow velocity pattern in Mode II for $Ek = 6{\cdot}10^{-4}$. The flow field is obtained for models No. 4 and 5 and is scaled so that $U = 0.21$ m/s (see Table 2.1). The velocity fields are averaged over at least 0.02 viscous diffusion times and longitude. The x-axis is given in non-dimensional radius, $\tilde{r} = (r - r_i)/D$, where $r_i = r_o - D$. The dashed lines mark the position of the tangent cylinder (the cylinder with radius r_i whose axis is identical with the rotation axis).

Model No.	N_r	j_{max}	Pr	Ek	Ra	Ro_{loc}	Ro_c	R_M	Nu	Ro
0	67	159	10.0	$6{\cdot}10^{-4}$	$3.34{\cdot}10^{6}$	5.86	0.35	1.78	16.56	0.04
1	73	177	10.0	$6{\cdot}10^{-4}$	$6.67{\cdot}10^{6}$	11.73	0.49	3.56	25.14	0.06
2	73	177	10.0	$6{\cdot}10^{-4}$	$1.00{\cdot}10^{7}$	17.59	0.60	5.33	31.45	0.08
3	73	177	10.0	$6{\cdot}10^{-4}$	$1.67{\cdot}10^{7}$	29.32	0.77	8.89	41.57	0.12
4	81	213	10.0	$6{\cdot}10^{-4}$	$2.33{\cdot}10^{7}$	41.05	0.92	12.45	47.42	0.19
5	81	237	10.0	$6{\cdot}10^{-4}$	$2.67{\cdot}10^{7}$	46.91	0.98	14.23	49.79	0.21
7	73	177	10.0	$3{\cdot}10^{-4}$	$1.09{\cdot}10^{7}$	6.35	0.31	1.78	24.48	0.04
8	73	177	10.0	$3{\cdot}10^{-4}$	$2.19{\cdot}10^{7}$	12.70	0.44	3.56	37.03	0.06
9	73	177	10.0	$3{\cdot}10^{-4}$	$3.28{\cdot}10^{7}$	19.04	0.54	5.33	45.98	0.08
10	85	237	10.0	$3{\cdot}10^{-4}$	$5.47{\cdot}10^{7}$	31.74	0.70	8.89	58.64	0.10
11	89	237	10.0	$3{\cdot}10^{-4}$	$6.57{\cdot}10^{7}$	38.09	0.77	10.67	62.59	0.14
12	89	297	10.0	$3{\cdot}10^{-4}$	$8.76{\cdot}10^{7}$	50.78	0.89	14.23	72.00	0.17
13	73	213	10.0	$1{\cdot}10^{-4}$	$1.80{\cdot}10^{7}$	1.80	0.13	0.44	14.43	0.01
14	73	213	10.0	$1{\cdot}10^{-4}$	$3.60{\cdot}10^{7}$	3.60	0.19	0.89	23.67	0.02
15	81	237	10.0	$1{\cdot}10^{-4}$	$7.20{\cdot}10^{7}$	7.20	0.27	1.78	41.02	0.04
16	89	285	10.0	$1{\cdot}10^{-4}$	$1.44{\cdot}10^{8}$	14.39	0.38	3.56	64.13	0.06
17	117	447	10.0	$1{\cdot}10^{-4}$	$2.16{\cdot}10^{8}$	21.59	0.46	5.33	71.48	0.09
18	81	237	10.0	$6{\cdot}10^{-5}$	$4.32{\cdot}10^{7}$	1.91	0.12	0.44	17.72	0.01
19	89	267	10.0	$6{\cdot}10^{-5}$	$8.64{\cdot}10^{7}$	3.81	0.18	0.89	30.29	0.03
20	89	317	10.0	$6{\cdot}10^{-5}$	$1.30{\cdot}10^{8}$	5.72	0.22	1.33	43.26	0.03
21	73	177	1.0	$6{\cdot}10^{-4}$	$3.34{\cdot}10^{5}$	2.33	0.35	1.00	2.80	0.06
22	73	177	1.0	$6{\cdot}10^{-4}$	$1.00{\cdot}10^{6}$	7.00	0.60	3.00	7.03	0.14
23	85	213	1.0	$6{\cdot}10^{-4}$	$1.67{\cdot}10^{6}$	11.67	0.77	5.00	9.78	0.20
24	85	213	1.0	$6{\cdot}10^{-4}$	$2.33{\cdot}10^{6}$	16.34	0.92	7.00	12.66	0.23
25	97	267	1.0	$6{\cdot}10^{-4}$	$3.34{\cdot}10^{6}$	23.35	1.10	10.00	15.11	0.38
26	85	213	1.0	$3{\cdot}10^{-4}$	$2.19{\cdot}10^{6}$	5.05	0.44	2.00	6.81	0.11
27	85	237	1.0	$3{\cdot}10^{-4}$	$5.47{\cdot}10^{6}$	12.64	0.70	5.00	14.85	0.17
28	85	213	1.0	$1{\cdot}10^{-4}$	$7.20{\cdot}10^{6}$	2.87	0.27	1.00	4.87	0.06
29	97	253	1.0	$1{\cdot}10^{-4}$	$2.16{\cdot}10^{7}$	8.60	0.46	3.00	16.26	0.12
30	97	253	1.0	$1{\cdot}10^{-4}$	$3.60{\cdot}10^{7}$	14.33	0.60	5.00	26.02	0.14
31	97	237	1.0	$6{\cdot}10^{-5}$	$1.73{\cdot}10^{7}$	3.04	0.25	1.00	7.45	0.06
32	73	177	3.0	$6{\cdot}10^{-4}$	$1.00{\cdot}10^{6}$	3.62	0.35	1.32	5.63	0.06
33	73	197	3.0	$6{\cdot}10^{-4}$	$3.00{\cdot}10^{6}$	10.87	0.60	3.95	13.76	0.12
34	85	213	3.0	$6{\cdot}10^{-4}$	$5.00{\cdot}10^{6}$	18.11	0.77	6.58	19.46	0.16
35	85	237	3.0	$6{\cdot}10^{-4}$	$7.00{\cdot}10^{6}$	25.36	0.92	9.21	23.85	0.20
36	97	267	3.0	$6{\cdot}10^{-4}$	$8.01{\cdot}10^{6}$	28.98	0.98	10.53	25.28	0.22
37	73	177	3.0	$3{\cdot}10^{-4}$	$3.28{\cdot}10^{6}$	3.92	0.31	1.32	8.53	0.06
38	85	213	3.0	$3{\cdot}10^{-4}$	$9.85{\cdot}10^{6}$	11.76	0.54	3.95	20.26	0.12
39	100	253	3.0	$3{\cdot}10^{-4}$	$1.64{\cdot}10^{7}$	19.61	0.70	6.58	26.97	0.15
40	73	213	3.0	$1{\cdot}10^{-4}$	$1.08{\cdot}10^{7}$	2.22	0.19	0.66	7.59	0.03
41	85	213	3.0	$1{\cdot}10^{-4}$	$2.16{\cdot}10^{7}$	4.45	0.27	1.32	16.47	0.05
42	97	253	3.0	$1{\cdot}10^{-4}$	$4.32{\cdot}10^{7}$	8.89	0.38	2.63	28.65	0.08
43	89	237	3.0	$6{\cdot}10^{-5}$	$2.59{\cdot}10^{7}$	2.36	0.18	0.66	9.49	0.03
44	97	285	3.0	$6{\cdot}10^{-5}$	$5.18{\cdot}10^{7}$	4.71	0.25	1.32	20.82	0.05

Table 2.2: List of numerical simulations used to derive the scaling laws (Eqs. 2.1 and 2.2). Symbols N_r and j_{max} denote the number of the Chebyshev points and the cut-off degree used to discretize the governing equations in the radial and lateral directions, respectively. The results of the simulations are represented by the Nusselt (Nu) and Rossby (Ro) numbers.

3 Radius ratio: 0.90

$$Ra = (4.23 \pm 0.01) Pr^{+1.27 \pm 0.01} Ek^{-2.19 \pm 0.01} Ra_Q^{0.62 \pm 0.01} \tag{3.1}$$

$$Ro = (0.38 \pm 0.02) Pr^{-0.01 \pm 0.01} Ek^{-0.20 \pm 0.02} Ra_Q^{0.39 \pm 0.01} \tag{3.2}$$

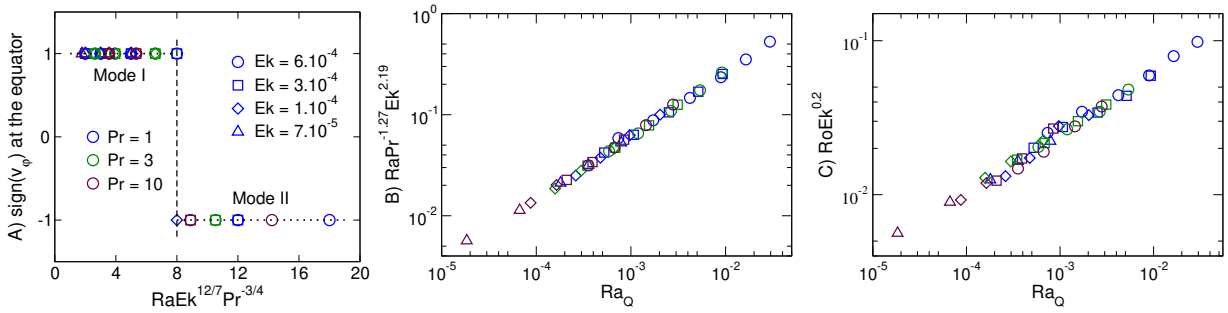

Figure 3.1: A) The sign of the zonal flow velocity on the outer boundary at the equator as a function of parameter $R_M = RaEk^{12/7}Pr^{-3/4}$. The overturn of equatorial zonal flow (vertical dashed line) is marked by $R_M \approx 8.0$. B) Graphs illustrating the scaling laws derived for Ra (Eq. 3.1) from the dataset in Table 3.2 using the least squares method. C) Graphs illustrating the scaling laws derived for Ro (Eq. 3.2) from the same dataset. Shapes and colors of the symbols indicate the values of parameters Ek and Pr used in the numerical simulation.

r_o [km]	D [km]	H [km]	Radius ratio	Ek	Ra_Q	Ra	U [m/s]
2500	119	134	0.95	$1.3{\cdot}10^{-11}$	$3.1{\cdot}10^{-8}$	$1.2{\cdot}10^{21}$	0.08
2477	24	157	0.99	$3.1{\cdot}10^{-10}$	$7.4{\cdot}10^{-7}$	$8.3{\cdot}10^{18}$	0.02

Table 3.1: Models of internal structure of Ganymede with aspect ratio 0.90 and higher [Vance et al., 2018]. r_o is the outer radius of the ocean, D is the thickness of the ocean and H denotes the thickness of the ice shell. U is dimensional rms velocity (Eq. 3.2). The ocean is situated in the transitional regime regardless the ocean thickness (D), as Ro_{loc} exceeds 10^3 and $Ro_c \leq 0.28$ in both cases. The flow geometry resembles Mode II, as $R_M \geq 50$ (see Fig 3.1A).

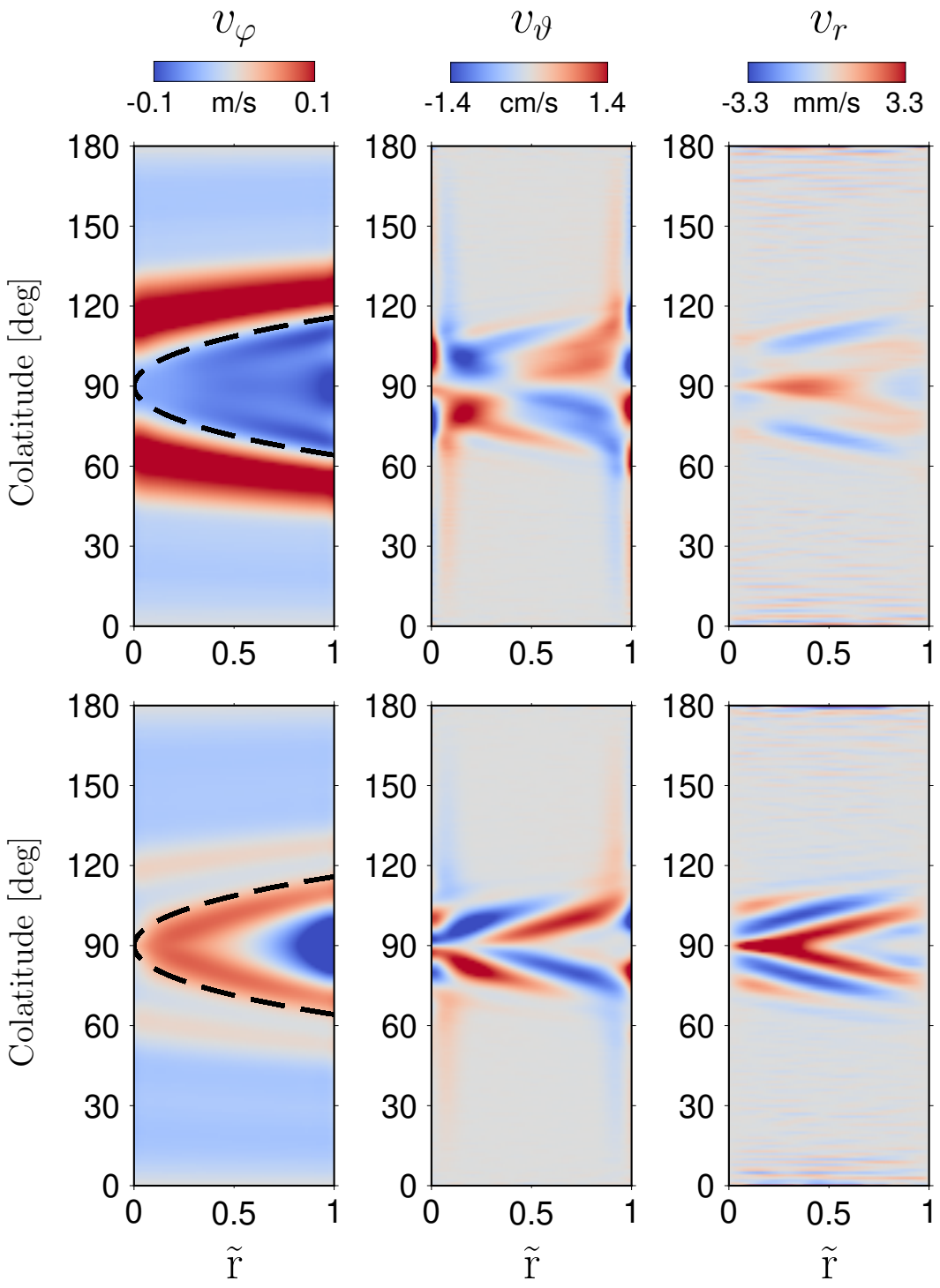

Figure 3.2: Forking of flow velocity pattern in Mode II for $Ek = 3{\cdot}10^{-4}$. The flow field is obtained for models No. 36 and 37 and is scaled so that $U = 0.08\,\mathrm{m/s}$ (see Table 3.1). The velocity fields are averaged over at least 0.02 viscous diffusion times and longitude. The x-axis is given in non-dimensional radius, $\tilde{r} = (r - r_i)/D$, where $r_i = r_o - D$. The dashed lines mark the position of the tangent cylinder (the cylinder with radius r_i whose axis is identical with the rotation axis).

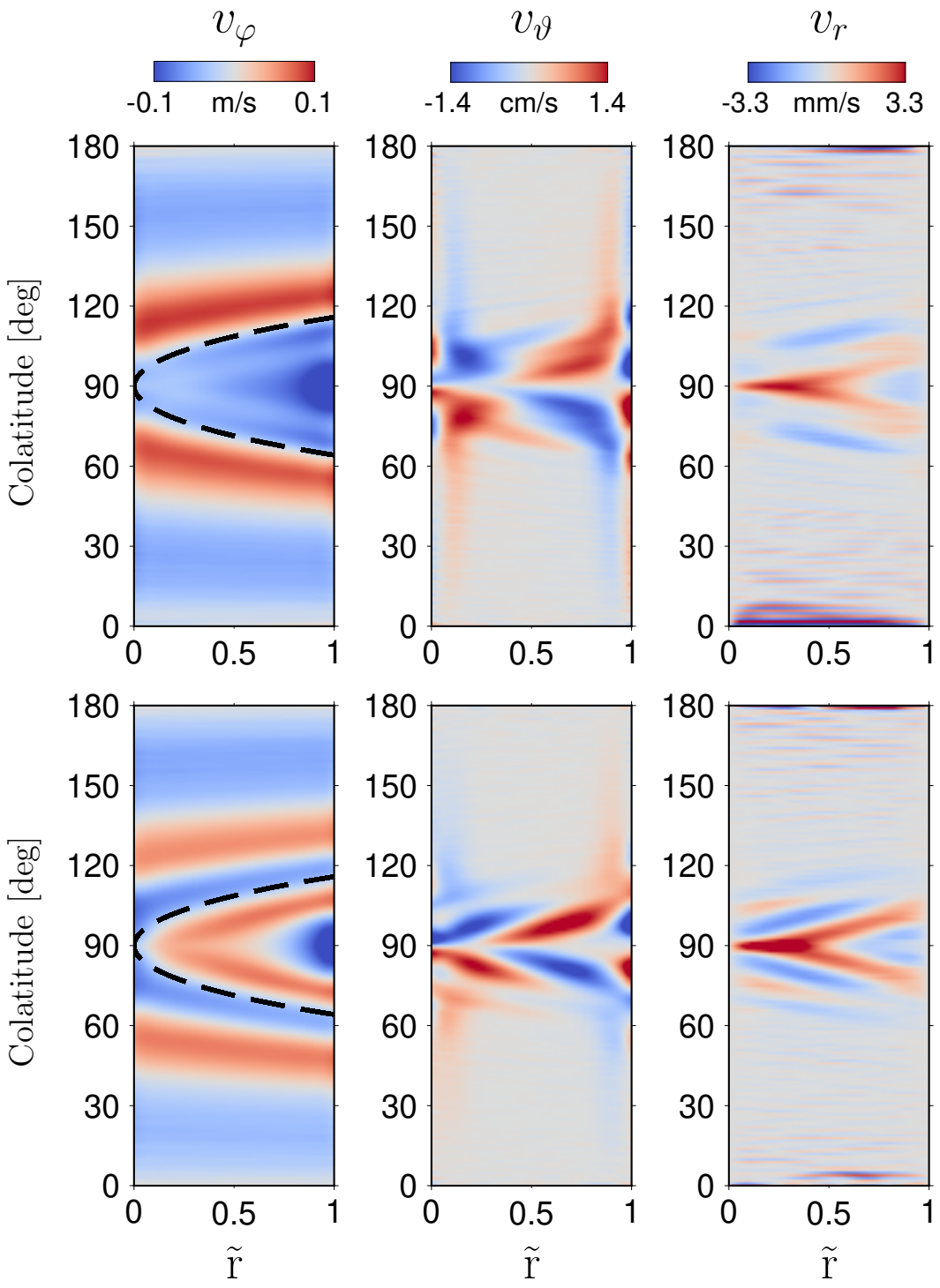

Figure 3.3: Forking of flow velocity pattern in Mode II for $Ek = 6{\cdot}10^{-4}$. The flow field is obtained for models No. 32 and 33 and is scaled so that $U = 0.08\,\mathrm{m/s}$ (see Table 3.1). The velocity fields are averaged over at least 0.02 viscous diffusion times and longitude. The x-axis is given in non-dimensional radius, $\tilde{r} = (r - r_i)/D$, where $r_i = r_o - D$. The dashed lines mark the position of the tangent cylinder (the cylinder with radius r_i whose axis is identical with the rotation axis).

Model No.	N_r	j_{max}	Pr	Ek	Ra	Ro_{loc}	Ro_c	R_M	Nu	Ro
1	61	157	1	$6{\cdot}10^{-4}$	$6.67{\cdot}10^{5}$	4.67	0.49	2.00	5.11	0.11
2	61	157	1	$6{\cdot}10^{-4}$	$1.00{\cdot}10^{6}$	7.00	0.60	3.00	7.95	0.15
3	73	177	1	$6{\cdot}10^{-4}$	$1.67{\cdot}10^{6}$	11.67	0.77	5.00	11.67	0.19
4	73	177	1	$6{\cdot}10^{-4}$	$2.67{\cdot}10^{6}$	18.68	0.98	8.00	15.49	0.26
5	73	207	1	$6{\cdot}10^{-4}$	$4.00{\cdot}10^{6}$	28.02	1.20	12.00	18.95	0.35
6	85	257	1	$6{\cdot}10^{-4}$	$6.00{\cdot}10^{6}$	42.02	1.47	18.00	22.68	0.43
7	73	177	1	$3{\cdot}10^{-4}$	$2.19{\cdot}10^{6}$	5.05	0.44	2.00	8.84	0.10
8	73	177	1	$3{\cdot}10^{-4}$	$3.28{\cdot}10^{6}$	7.58	0.54	3.00	12.09	0.14
9	73	207	1	$3{\cdot}10^{-4}$	$5.47{\cdot}10^{6}$	12.64	0.70	5.00	17.05	0.17
10	81	237	1	$3{\cdot}10^{-4}$	$8.76{\cdot}10^{6}$	20.22	0.89	8.00	21.78	0.22
11	81	285	1	$3{\cdot}10^{-4}$	$1.31{\cdot}10^{7}$	30.32	1.09	12.00	26.29	0.30
12	73	217	1	$1{\cdot}10^{-4}$	$1.44{\cdot}10^{7}$	5.73	0.38	2.00	18.17	0.08
13	73	247	1	$1{\cdot}10^{-4}$	$2.16{\cdot}10^{7}$	8.60	0.46	3.00	22.01	0.11
14	73	377	1	$1{\cdot}10^{-4}$	$3.60{\cdot}10^{7}$	14.33	0.60	5.00	27.00	0.18
15	97	413	1	$1{\cdot}10^{-4}$	$5.76{\cdot}10^{7}$	22.92	0.76	8.00	35.32	0.21
16	81	257	1	$7{\cdot}10^{-5}$	$2.65{\cdot}10^{7}$	5.97	0.36	2.00	19.80	0.08
17	81	257	1	$7{\cdot}10^{-5}$	$3.98{\cdot}10^{7}$	8.95	0.44	3.00	25.98	0.11
18	73	347	1	$7{\cdot}10^{-5}$	$6.63{\cdot}10^{7}$	14.92	0.57	5.00	34.69	0.15
19	65	177	3	$6{\cdot}10^{-4}$	$2.00{\cdot}10^{6}$	7.25	0.49	2.63	12.23	0.09
20	65	177	3	$6{\cdot}10^{-4}$	$3.00{\cdot}10^{6}$	10.87	0.60	3.95	16.54	0.12
21	73	197	3	$6{\cdot}10^{-4}$	$5.00{\cdot}10^{6}$	18.11	0.77	6.58	22.13	0.15
22	73	197	3	$6{\cdot}10^{-4}$	$8.01{\cdot}10^{6}$	28.98	0.98	10.53	27.96	0.21
23	73	227	3	$3{\cdot}10^{-4}$	$6.57{\cdot}10^{6}$	7.84	0.44	2.63	17.69	0.09
24	73	227	3	$3{\cdot}10^{-4}$	$9.85{\cdot}10^{6}$	11.76	0.54	3.95	23.17	0.11
25	73	227	3	$3{\cdot}10^{-4}$	$1.64{\cdot}10^{7}$	19.61	0.70	6.58	31.55	0.15
26	85	267	3	$3{\cdot}10^{-4}$	$2.63{\cdot}10^{7}$	31.37	0.89	10.53	39.57	0.20
27	85	267	3	$1{\cdot}10^{-4}$	$4.32{\cdot}10^{7}$	8.89	0.38	2.63	32.96	0.08
28	85	267	3	$1{\cdot}10^{-4}$	$6.48{\cdot}10^{7}$	13.34	0.46	3.95	41.45	0.10
29	85	297	3	$1{\cdot}10^{-4}$	$1.08{\cdot}10^{8}$	22.23	0.60	6.58	55.25	0.14
30	73	177	10	$6{\cdot}10^{-4}$	$6.67{\cdot}10^{6}$	11.73	0.49	3.56	24.68	0.07
31	85	237	10	$6{\cdot}10^{-4}$	$1.00{\cdot}10^{7}$	17.59	0.60	5.33	30.99	0.08
32	85	237	10	$6{\cdot}10^{-4}$	$1.67{\cdot}10^{7}$	29.32	0.77	8.89	40.08	0.12
33	97	267	10	$6{\cdot}10^{-4}$	$2.67{\cdot}10^{7}$	46.91	0.98	14.23	48.36	0.16
34	85	237	10	$3{\cdot}10^{-4}$	$2.19{\cdot}10^{7}$	12.70	0.44	3.56	35.50	0.06
35	85	237	10	$3{\cdot}10^{-4}$	$3.28{\cdot}10^{7}$	19.04	0.54	5.33	44.27	0.09
36	97	285	10	$3{\cdot}10^{-4}$	$5.47{\cdot}10^{7}$	31.74	0.70	8.89	57.30	0.14
37	97	321	10	$3{\cdot}10^{-4}$	$8.50{\cdot}10^{7}$	49.30	0.87	13.81	68.21	0.16
38	97	267	10	$1{\cdot}10^{-4}$	$1.44{\cdot}10^{8}$	14.39	0.38	3.56	60.53	0.06
39	97	267	10	$1{\cdot}10^{-4}$	$2.16{\cdot}10^{8}$	21.59	0.46	5.33	75.77	0.08
40	97	285	10	$7{\cdot}10^{-5}$	$1.33{\cdot}10^{8}$	7.50	0.25	1.78	40.45	0.04
41	113	321	10	$7{\cdot}10^{-5}$	$2.65{\cdot}10^{8}$	14.99	0.36	3.56	73.29	0.06

Table 3.2: List of numerical simulations used to derive the scaling laws (Eqs. 3.1 and 3.2). Symbols N_r and j_{max} denote the number of the Chebyshev points and the cut-off degree used to discretize the governing equations in the radial and lateral directions, respectively. The results of the simulations are represented by the Nusselt (Nu) and Rossby (Ro) numbers.

References

H.C.F.C. Hay and I. Matsuyama. Nonlinear tidal dissipation in the subsurface oceans of Enceladus and other icy satellites. *Icarus*, 319:68–85, 2019. doi: 10.1016/j.icarus.2018.09.019.

J. Kvorka and O. Čadek. A numerical model of convective heat transfer in Titan's subsurface ocean. *Icarus*, 376:114853, 2022. doi: 10.1016/j.icarus.2021.114853.

K. M. Soderlund. Ocean dynamics of outer solar system satellites. *Geophys. Res. Lett.*, 46:8700–8710, 2019. doi: 10.1029/2018GL081880.

S. D. Vance, M. P. Panning, S. Stähler, F. Cammarano, B. G. Bills, G. Tobie, S. Kamata, S. Kedar, C. Sotin, W. T. Pike, R. Lorenz, H.-H. Huang, J. M. Jackson, and B. Banerdt. Geophysical investigations of habitability in ice-covered ocean worlds. *J. Geophys. Res.: Planets*, 123:180–205, 2018. doi: 10.1002/2017JE005341.